This article has been accepted for publication in IEEE Transactions on Power Delivery. This is the author's version which has not been fully edited and content may change prior to final publication. Citation information: DOI 10.1109/TPWRD.2022.3218658

Use of Inverter-based Air Conditioners to Provide Voltage Regulation Services in Unbalanced Distribution Networks

Yongzhu Hua, Qiangqiang Xie*, Hongxun Hui, Yi Ding, Jiadong Cui, Lihuan Shao

Abstract—**The large-scale integration of photovoltaic generation and electric vehicles results in over-voltage, under-voltage, and voltage unbalance problems in three-phase distribution networks. The power consumption of the air conditioners (ACs) is large among the daily electrical appliances and can be regulated to provide voltage regulation services. To protect occupants' privacy and utilize the existing dispatch strategy of the battery, we propose a thermal battery equivalent model of the inverter-based AC to regulate the active power and provide a voltage regulation service. Moreover, an improved Newton-Raphson power-flow algorithm is developed to reduce the computational burden. The affinity propagation method is applied to cluster ACs according to different operating states. Thus, the ACs' operating frequencies are adjusted to reset the corresponding operating power. The feasibility of the thermal battery equivalent model and voltage regulation algorithm is verified based on case studies utilizing the revised IEEE 33-node three-phase power distribution network.**

Index Terms—**air conditioners (ACs); affinity propagation; unbalanced load; thermal battery model.**

I. INTRODUCTION

The development of distributed energy resources (DERs) and the popularization of electric vehicles (EVs) can promote sustainable development and construction of a low-carbon society. As the single-phase penetration of DERs increases, the imbalance connection of single-phase lines, intermittent DER output, and randomness of EV charging behavior cause significant challenges to distribution networks, which result in three-phase unbalanced voltage [1], over-voltage, and under-voltage [2]. Therefore, voltage regulation services are becoming increasingly crucial in distribution networks. Conventionally, voltage regulation methods primarily focus on the traditional reactive power regulation equipment [3][4][5] to eliminate voltage fluctuations and imbalances. The on-load tap changer (OLTC) can adjust the transformer voltage ratio in response to voltage fluctuations [6]. By continuously monitoring voltage and load current, the step-voltage regulator (SVR) can change the tap position for reactive power regulation to deal with voltage problems [7]. Besides, the capacitor banks (CBs) can provide reactive current, decrease the current from the source to the location of the CB, which will resolve the problem of the line voltage drop [8]. However, when three-phase unbalanced voltage, under-voltage, and over-voltage problems occur frequently, the OLTC, SVR, and CBs must be regulated continually. The maintenance costs will increase, and the service life of these regulation devices will decrease. More importantly, these traditional voltage regulation devices cannot respond rapidly to fast voltage variations. Providing reasonable reactive power can improve the operating voltage level and power supply quality of the power system. However, compared with the transmission network, the R/X ratio is much larger in the distribution networks, which causes reactive power regulation to be less effective. In addition, line congestion and power loss become severe when excessive reactive power is injected into low-voltage distribution networks [9]. To address the above problem, increasing focus is being given to regulate active power in distribution networks [10]. Adjusting active power does not require to interrupt the power supply and provide an effective method of solving the voltage problem to guarantee the electricity quality of consumers [11].

Demand response is an effective technology for rescheduling occupants' energy consumption to provide active power [12]. The traditional voltage regulation equipment cannot respond rapidly to voltage regulation, but demand response can utilize flexible loads on the user side to provide timely voltage regulation service. In this way, the demand response can solve the voltage regulation by shifting the power demands in the over-voltage/under-voltage periods. In recent years, information and communication technology has developed rapidly, the load can achieve remote control to participate in ancillary services [13]. The power usage of the load can be shifted momentarily, which makes demand-side management (DSM) excellent for exploiting the potential of improving

This work was supported by China Postdoctoral Science Foundation (2022M710039).

This paragraph of the first footnote will contain the date on which you submitted your paper for review. (Corresponding author: Qiangqiang Xie)

Y. Hua, Q. Xie, J. Cui, and L. Shao, are with the College of Electronics and Information, Hangzhou Dianzi University (e-mail: huayongzhu@hdu.edu.cn; xqq@hdu.edu.cn; cjd@hdu.edu.cn; slh@hdu.edu.cn).

H. Hui, is with the State Key Laboratory of Internet of Things for Smart City, Department of Electrical and Computer Engineering, University of Macau (e-mail: hongxunhui@um.edu.mo).

Y. Ding, is with the College of Electrical Engineering, Zhejiang University (e-mail: yiding@zju.edu.cn).

power system reliability [14], reducing the peak load demand [15], and saving electricity bills [16]. DSM is a response system that can monitor and remotely control flexible loads to promote the efficient use of energy in distribution networks [17]. Therefore, the DSM contributes significantly to improve the power quality of the distribution network [18]. The development of building insulation technology makes the thermal inertia of the building better to store the heat generated by the ACs for a longer time. When the AC's power consumption is regulated, the temperature variation has little impact on the occupant's thermal comfortness [19]. Besides, among all the demand response resources, ACs have become more widespread and account for a massive proportion of the daily load. The ACs can participate in the auxiliary services of the power system through demand response. In contrast to single-speed ACs, the inverter-based AC (IAC) can continuously regulate the compressor's speed [20]. Demand response can enable consumers to adjust IACs' power consumption through load curtailment, shift the power consumption over time, or generate and store energy at certain times to participate in auxiliary services with more flexibility [21]. In summary, the distribution characteristics and power consumption of AC makes it has great potential for voltage regulation through demand response.

Under the premise of guaranteeing the room temperature in a comfortable range, the AC can flexibly regulate its operating power to provide active power and follow voltage regulation instructions. To research the potential of AC's voltage regulation, a thermoelectric equivalent model is developed to describe the thermal dynamic variation of the room and the performance of the active power provided by ACs. The IAC can be equivalent to a battery in the thermoelectric model. Thus, the existing battery energy storage system (BESS) can send regulation instructions to control the IACs, making it feasible for IACs to provide voltage regulation services. Moreover, when the thermoelectric equivalent model is applied in regulation, the occupants are not required to provide their room temperatures directly; therefore, their privacy is protected. To calculate the voltage and regulation power of each node in a three-phase distribution network, an improved Newton-Raphson power-flow method is developed. The proposed method can reduce the iteration time of the Newton-Raphson algorithm. To guarantee the occupants' comfortness, the affinity propagation (AP) algorithm is used to classify the ACs based on the state of thermal energy storage. The ACs in different clusters change operating power to provide various active powers. The main contributions of this paper are as follows:

1. A thermoelectric equivalent model of the IAC to provide a voltage regulation service is developed. Based on this model, the thermal dynamic variation of the room and the performance of the active power provided by ACs can be described.
2. The IAC is equivalent to a traditional battery. Thus, the IAC can be controlled and compatible with the existing dispatch model of the BESS, which can protect occupants' privacy.
3. An improved Newton-Raphson power-flow algorithm is developed to obtain the nodal voltage and regulation power. This method consumes less calculation time than the traditional Newton-Raphson power-flow method.
4. The AP algorithm is utilized to cluster AC according to the state of thermal energy storage. Different clusters of ACs regulate the operating frequencies to provide different active powers for voltage regulation.

The rest of the paper is organized as follows: Section II introduces the system architecture of the aggregation model, Section III develops the thermoelectric model of the IACs, Section IV develops the three-phase power flow optimization, and Section V introduces the AC clustering and power mismatch allocation. Simulation results of the thermal battery equivalent model and voltage regulation algorithm are discussed in Section VI, and a conclusion is drawn in Section VII.

II. THE SYSTEM ARCHITECTURE OF THE AGGREGATION MODEL

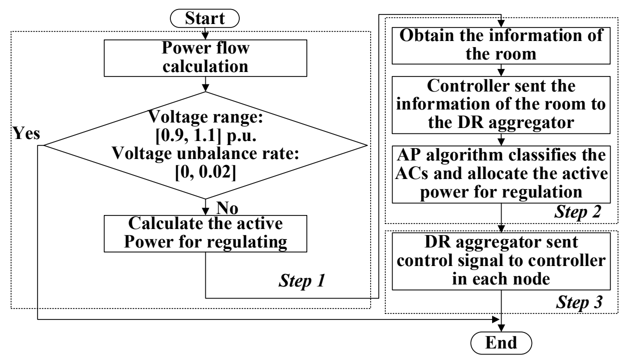

Fig. 1 Flow chart of the AC providing the voltage regulation service

As shown in Fig. 1, using IACs to provide voltage regulation services comprises three steps: 1) Calculating the power-flow: the power-flow of the distribution network is calculated by the Newton-Raphson method. 2) Obtaining the room information and classifying the ACs: room information is obtained by using the thermoelectric model. 3) Allocating the active power for regulation: according to the AC information, the AP algorithm classifies the ACs and allocates the active power for voltage regulation. Finally, the voltage regulation signal is sent to the controller.

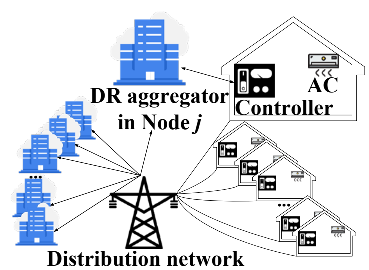

Fig. 2 Control structure for the ACs

The development of 5G technology and the Internet of Things provides advanced infrastructure for demand response (DR), which expedites the remote control of ACs [17]. The control structure comprises the distribution network, DR aggregators, smart controllers, and ACs. The controller shares the functions of communication, sensor, and control. The room temperature is obtained by collecting the data of the sensors' thermistors. The narrowband internet of things is also integrated into smart controllers to communicate with the DR aggregator. DR programs will be implemented to aggregate the ACs (energy management systems [18]) for voltage regulation when

This article has been accepted for publication in IEEE Transactions on Power Delivery. This is the author's version which has not been fully edited and content may change prior to final publication. Citation information: DOI 10.1109/TPWRD.2022.3218658

voltage problems occur in the distribution network. In the process of voltage optimization, the distribution system sends power-flow information to the DR aggregators in each node. In addition, the information of the room (the total energy consumption, the individual consumption of the ACs, and the indoor environmental parameters) will be feedback to the aggregator. According to the power-flow information sent from the distribution system, the aggregator decides whether the ACs need to provide the ancillary services. The controller receives the regulation signal to reset the set temperature of the ACs, which changes the operation power to provide active power for voltage regulation. Here, when the ACs' set temperature is adjusted, the room temperature should be within the maximum acceptable range to guarantee the comfortness of occupants. The system architecture is shown in Fig. 2.

III. Thermoelectric Model of IACs

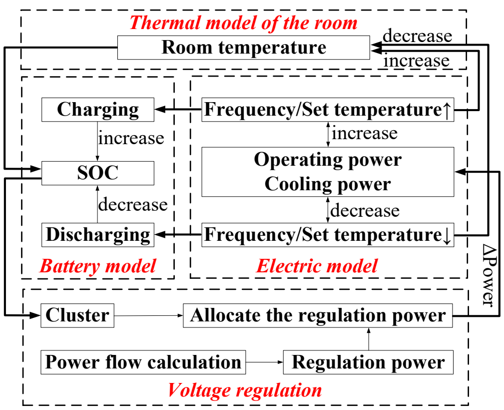

Fig. 3. Thermoelectric model of the IAC

To obtain the temperature information of the room, developing a thermoelectric model for the IAC is crucial. Fig. 3 shows a thermoelectric model, including the thermal model of the air-conditioned room and the electric model of the IAC. The thermal and electric models are used to evaluate the room temperature variation when the AC provides voltage regulation service. In addition, to improve the practicability of IACs to provide voltage regulation services, the IAC is regarded as a battery, which can protect occupants' privacy and utilize the existing dispatch strategy of battery [22]. The battery model can estimate the voltage regulation potential of AC and allocate the voltage regulation power to the AC based on the clustering results.

A. Thermal model of a room

The thermal model of an air-conditioned room can be used to formulate the thermal dynamic variation of the room and the operating power of the IAC. The dynamic behaviors of the air-conditioned room can be expressed as follows [23]:

$$Ca\frac{\mathrm{d}T_{\mathrm{in}}}{\mathrm{d}t}=\frac{(T_{\mathrm{out}}-T_{\mathrm{in}})}{R}+P_{\mathrm{cool}}'-P_{\mathrm{cool}} \tag{1}$$

where Ca is the heat capacity of air (J/°C); T_{in} and T_{out} are the temperature in the room (°C) and out the room (°C), respectively; R is the equivalent thermal resistance of an air-conditioned room (°C/W); P_{cool} is the cooling power made by the IAC (W); P_{cool}' is the equivalent heat rate of the other factors (W).

The differential equation (1) can be transformed to obtain the real-time room temperature:

$$T_{\mathrm{in}}(t)=(T_{\mathrm{in}}(t\text{-}\Delta t)\text{-}T_{\mathrm{out}}(t)\text{-}RP_{\mathrm{cool}}'+RP_{\mathrm{cool}}(t))e^{-\frac{\Delta t}{RCa}}+T_{\mathrm{out}}(t)+RP_{\mathrm{cool}}'\text{-}RP_{\mathrm{cool}}(t) \tag{2}$$

where Δt is the time interval, which was set to 30 s in this study.

B. Electric model of the IAC

The electric model can formulate the performance of the active power provided by the IACs. By controlling the operating frequency of the compressor, the IAC can regulate the operating power. According to the difference between the room and set temperature, the compressor changes the operating frequency to keep the room temperature at the set temperature. Therefore, the active power can be provided by resetting the set temperature to change the operating frequency of the compressor, which can be expressed as follows [24]:

$$\begin{cases} f_{\mathrm{AC}}=180, & T_{\mathrm{in}}\text{-}T_{\mathrm{set}}\geq 2 \\ f_{\mathrm{AC}}=50\cdot(T_{\mathrm{in}}\text{-}T_{\mathrm{set}})+80, & \text{-}1\leq T_{\mathrm{in}}\text{-}T_{\mathrm{set}}<2 \\ f_{\mathrm{AC}}=30, & T_{\mathrm{in}}\text{-}T_{\mathrm{set}}<\text{-}1 \end{cases} \tag{3}$$

where f_{AC} is the operating frequency of the compressor (Hz), which is between $f_{\mathrm{AC}}^{\mathrm{min}}$ and $f_{\mathrm{AC}}^{\mathrm{max}}$ Hz. When T_{in}-T_{set} decreases by 1 °C, the operating frequency increases 50 Hz.

The operating and cooling power can be regulated by resetting the operating frequency of the compressor, which can be expressed as:

$$P_{\mathrm{cool}}=SW_{\mathrm{AC}}\cdot(a\cdot f_{\mathrm{AC}}^{2}+b\cdot f_{\mathrm{AC}}+c) \tag{4}$$

$$P_{\mathrm{operation}}=SW_{\mathrm{AC}}\cdot(m\cdot f_{\mathrm{AC}}+n) \tag{5}$$

where SW_{AC} expresses the switch status of the IAC; P_{cool} is the IAC's cooling power; a, b, and c are the coefficients of the cooling power equation; $P_{\mathrm{operation}}$ is the IAC's operating power (W); and m and n are the coefficients of the operating power equation. When the AC works in the refrigeration state, a large proportion of $P_{\mathrm{operation}}$ is transformed to P_{cool} to transfer heat from the room to the external environment. The relationship between P_{cool} and $P_{\mathrm{operation}}$ can be described by the energy efficiency ratio, which can be expressed as

$$EER=\frac{P_{\mathrm{cool}}}{P_{\mathrm{operation}}} \tag{6}$$

The compressor of the IAC changes its operating frequency according to the room and set temperatures. When the room temperature attains the set value, the compressor operates at a certain frequency to maintain room temperature. The cooling and operating power can be expressed as:

$$P_{\mathrm{cool\_base}}=\frac{(T_{\mathrm{out}}\text{-}T_{\mathrm{set}})}{R}+P_{\mathrm{cool}}' \tag{7}$$

$$P_{\mathrm{op\_base}}=n+\frac{\text{-}b\cdot m\cdot R+m\cdot\sqrt{b^{2}\cdot R^{2}\text{-}4a\cdot R\cdot(c\cdot R\text{-}T_{\mathrm{out}}+T_{\mathrm{set}}\text{-}P_{\mathrm{cool}}'\cdot R)}}{2a\cdot R} \tag{8}$$

where $P_{\mathrm{cool\_base}}$ and $P_{\mathrm{op\_base}}$ are the cooling power (W) and operating power (W), respectively, which can keep the room temperature at the set temperature.

C. Battery model of the IAC

This article has been accepted for publication in IEEE Transactions on Power Delivery. This is the author's version which has not been fully edited and content may change prior to final publication. Citation information: DOI 10.1109/TPWRD.2022.3218658

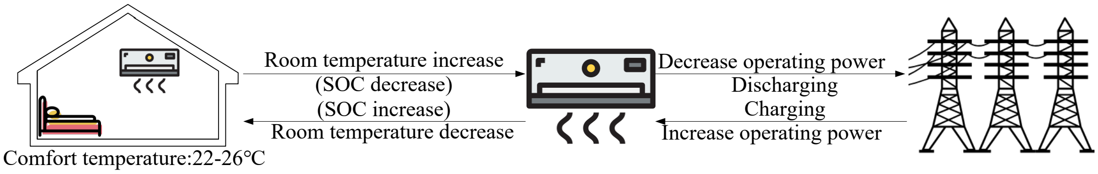

Fig. 4 Battery model of the IAC

The battery model can avoid violating occupants' privacy and is compatible with the existing dispatch model of the existing battery storage energy system, which is similar to the battery and has certain heat storage characteristics. The performance characteristics of the battery model are shown in Fig. 4. By regulating the set temperature, the AC can decrease or increase the operating power, which is equivalent to the discharging/charging process. When the set temperature changes, the room temperature will increase or decrease, which is similar to the variation in the battery's state of charge (SOC). IACs can convert electrical energy to heat energy and store it in an air-conditioned room for a certain time. During the regulation period, the room temperature should be maintained at 22–26 °C to guarantee the comfortness of occupants. Therefore, the maximum heat storage capacity of the air-conditioned room can be described by [25]:

$$H_{\max}=Ca\cdot(T_{\max}\text{-}T_{\min}) \tag{9}$$

where $H_{\max}$ is the maximum capacity of thermal energy (J) stored in the air-conditioned room; $[T_{\max}, T_{\min}]$ indicates the comfortable temperatures of the room for occupants.

Similar to a battery's SOC, the SOC of an air-conditioned room can also be used to describe the room for thermal energy storage [22]. The SOC of the air-conditioned room can be expressed as:

$$\rho_{\mathrm{SOC\_AC}_i}=\frac{T_{\max}\text{-}T_{\mathrm{in}}}{T_{\max}\text{-}T_{\min}}=\rho_{\mathrm{SOC\_AC}_i}{}'\text{-}\frac{\Delta T_{\mathrm{in}}}{T_{\max}\text{-}T_{\min}} \tag{10}$$

where $\rho_{\mathrm{SOC\_AC}_i}$ and $\rho_{\mathrm{SOC\_AC}_i}{}'$ are the states of thermal energy storage at current and previous time slots, respectively; ΔT_{in} is the difference in room temperature between two-time slots.

When the room temperature attains the set value, the cooling power is $P_{\mathrm{cool\_base}}$, and the room temperature is stable. When the IAC gets the regulation signal, the active power will be provided for the distribution network, and the current cooling power and operating power can be expressed as:

$$P_{\mathrm{cool\_current}}=P_{\mathrm{cool\_base}}\text{-}\Delta P_{\mathrm{cool}} \tag{11}$$

$$P_{\mathrm{operation\_current}}=\frac{2a\cdot n\text{-}m\cdot b\text{-}m\cdot\sqrt{b^2\text{-}4a\cdot(c\text{-}P_{\mathrm{cool\_current}})}}{2a} \tag{12}$$

where $P_{\mathrm{cool\_current}}$ and $P_{\mathrm{operation\_current}}$ are the cooling and operating powers (W) of the AC at the current time slot, respectively; ΔP_{cool} is the variation in the cooling power when the AC provides active power.

When the regulation signal is received, the operating frequency is reset, which can be expressed as:

$$\Delta f(t)=f(t)\text{-}f(t\text{-}1)=\frac{\Delta P_{\mathrm{operation}}}{m} \tag{13}$$

$$\begin{cases} P_{\mathrm{ch}}=\Delta P_{\mathrm{operation}}, & \Delta f>0 \\ P_{\mathrm{disch}}=\Delta P_{\mathrm{operation}}, & \Delta f<0 \end{cases} \tag{14}$$

where $\Delta P_{\mathrm{operation}}$ is the active power provided by the AC. When the compressor's operating frequency increases, the operating power increases, $\Delta P_{\mathrm{operation}}$ is positive, and the state of the AC is equivalent to charging. The room temperature decreases and $\rho_{\mathrm{SOC\_AC}_i}$ increases. When the compressor's operating frequency decreases, the operating power decreases, $\Delta P_{\mathrm{operation}}$ is negative, and the state of the AC is equivalent to discharging. The room temperature increases and $\rho_{\mathrm{SOC\_AC}_i}$ decreases. When $P_{\mathrm{cool\_current}} \neq P_{\mathrm{cool\_base}}$, the room temperature rises or falls, and the set temperature cannot be maintained. The change in room temperature can be expressed as:

$$\Delta T_{\mathrm{in}}=\text{-}R\cdot\Delta P_{\mathrm{cool}} \tag{15}$$

In addition, the room temperature must be maintained at 22–26 °C to avoid affecting the occupant's comfortness [26].

IV. THREE-PHASE POWER-FLOW OPTIMIZATION

The power-flow calculation of the power system is usually solved using the Newton-Raphson algorithm [27]. Compared with the conventional Newton-Raphson algorithm, this study proposes an improved Newton-Raphson algorithm for a three-phase distribution network power-flow calculation, which shortens the computation time and improves the robustness to respond to the load fluctuation and R/X ratio.

The improved Newton-Raphson algorithm can be used to calculate the power flow of the low-voltage distribution network with the short distribution line segments. Owing to the small impedance between some nodes, the voltage difference between these nodes and power-flow can be neglected [28][29]. Therefore, the nodal voltage and phase angle can be expressed as follows:

$$|U_k^s| \cong |U_j^s|;\theta_k^s \cong \theta_j^s;\theta_k^s\text{-}\theta_j^s=\theta_{kj}^s=0 \tag{16}$$

where U_k^s is the voltage at node k of phase s (p.u.); s={A, B, C}; θ_k^s is the phase angle at node k of phase s (°); θ_{kj}^s is their difference.

According to (16), the diagonal and off-diagonal elements in the Jacobian matrix $H_{kj}^s=\partial P_k^s/\partial\theta_j^s$, $N_{kj}^s=(\partial P_k^s/\partial U_j^s)U_j^s$, $J_{kj}^s=\partial Q_k^s/\partial\theta_j^s$, $L_{kj}^s=(\partial Q_k^s/\partial U_j^s)U_j^s$ can be transformed separately [28], which are shown in TABLE I.

TABLE I
DIAGONAL ELEMENTS AND THE OFF-DIAGONAL ELEMENTS JACOBIAN MATRIX

	DIAGONAL ELEMENTS	OFF-DIAGONAL ELEMENTS
H_{kj}^s	$\frac{\partial P_k^s}{\partial\theta_k^s}\cong\text{-}U_k^s\sum_{j=1,j\neq i}^{j=N}U_j^s CE_{kj}^s\cos\theta_{kj}^s$	$\frac{\partial P_k^s}{\partial\theta_j^s}\cong U_k^s U_j^s CE_{kj}^s\cos\theta_{kj}^s$
N_{kj}^s	$\frac{\partial P_k^s}{\partial U_k^s}U_k^s\cong\text{-}U_k^s\sum_{j=1,j\neq i}^{j=N}U_j^s SE_{kj}^s\cos\theta_{kj}^s$	$\frac{\partial P_k^s}{\partial U_j^s}U_j^s\cong\text{-}U_k^s U_j^s SE_{kj}^s\cos\theta_{kj}^s$
J_{kj}^s	$\frac{\partial Q_k^s}{\partial\theta_k^s}\cong\text{-}U_k^s\sum_{j=1,j\neq i}^{j=N}U_j^s SE_{kj}^s\cos\theta_{kj}^s$	$\frac{\partial Q_k^s}{\partial\theta_j^s}\cong U_k^s U_j^s SE_{kj}^s\cos\theta_{kj}^s$
L_{kj}^s	$\frac{\partial Q_k^s}{\partial U_k^s}U_k^s\cong U_k^s\sum_{j=1,j\neq i}^{j=N}U_j^s CE_{kj}^s\cos\theta_{kj}^s$	$\frac{\partial Q_k^s}{\partial U_j^s}U_j^s\cong U_k^s U_j^s CE_{kj}^s\cos\theta_{kj}^s$

In TABLE I, P_k^s and Q_k^s are the active and reactive powers at node k of phase s, respectively. CE_{kj}^s and SE_{kj}^s are the conductance and susceptance between nodes k and j of the phase s.

According to TABLE I, the Jacobian matrix can be simplified and inversed, which can be expressed as [29]:

$$IJ=\begin{bmatrix} H & N \\ J & L \end{bmatrix}^{-1}=\begin{bmatrix} E & [0] \\ [0] & E \end{bmatrix}^{-1}\begin{bmatrix} D_{CE} & -D_{SE} \\ D_{SE} & D_{CE} \end{bmatrix}^{-1}\begin{bmatrix} E^{\mathrm{T}} & [0] \\ [0] & E^{\mathrm{T}} \end{bmatrix}^{-1} =\begin{bmatrix} S_{\theta P} & S_{\theta Q} \\ S_{UP} & S_{UQ} \end{bmatrix} \tag{17}$$

$$\begin{bmatrix} \Delta\theta \\ \Delta U \end{bmatrix}=IJ\begin{bmatrix} \Delta P \\ \Delta Q \end{bmatrix} \tag{18}$$

where E is the element-node incident matrix that describes the incidence elements of nodes [29]. The diagonal matrices D_{CE} and D_{SE}consist of$U_k^s U_j^s CE_{kj}^s \cos\theta_{kj}^s$ and $U_k^s U_j^s SE_{kj}^s \cos\theta_{kj}^s$.

The nodal voltage and phase angle can be expressed as:

$$\Delta U=S_{UP}\cdot\Delta P+S_{UQ}\cdot\Delta Q \tag{19}$$

$$\Delta\theta=S_{\theta P}\cdot\Delta\theta+S_{\theta Q}\cdot\Delta\theta \tag{20}$$

The mismatch power at each time slot is given as:

$$\begin{aligned} \Delta P&=S_{UP}{}^{-1}\cdot\varepsilon_{\mathrm{P}}\cdot\Delta U \\ \Delta Q&=S_{UQ}{}^{-1}\cdot\varepsilon_{\mathrm{Q}}\cdot\Delta U \end{aligned} \tag{21}$$

In the above equations, $\Delta P=\left[\Delta P_1^{\mathrm{A}},...\Delta P_M^{\mathrm{A}}, \Delta P_1^{\mathrm{B}},...\Delta P_M^{\mathrm{B}}, \Delta P_1^{\mathrm{C}},...\Delta P_M^{\mathrm{C}}\right]^{\mathrm{T}}$, which describes nodal active power of each phase, and $\Delta U=\left[\Delta U_1^{\mathrm{A}},...\Delta U_M^{\mathrm{A}}, \Delta U_1^{\mathrm{B}},...\Delta U_M^{\mathrm{B}}, \Delta U_1^{\mathrm{C}},...\Delta U_M^{\mathrm{C}}\right]^{\mathrm{T}}$, which describes the nodal voltage of each phase.

Except under- and over-voltage problems, the voltage unbalance also deteriorates the power supply quality. Based on the IEEE Std. 112 (1991), the voltage unbalance rate is defined as the ratio of the maximum deviation of a voltage from the average voltage to the average voltage (MDV) [30]. The unbalance ratio can be expressed as:

$$\begin{cases} U_k^{\max}=\mathrm{Max}(\left|U_k^{\mathrm{A}}-U_k^{\mathrm{mean}}\right|,\left|U_k^{\mathrm{B}}-U_k^{\mathrm{mean}}\right|,\left|U_k^{\mathrm{C}}-U_k^{\mathrm{mean}}\right|) \\ \gamma_{\mathrm{MDV}\_k}=\dfrac{U_k^{\max}}{U_k^{\mathrm{mean}}} \end{cases} \tag{22}$$

where $U_k^{\max}$is the maximum deviation of the voltage from the average voltage; U_k^{mean} is the mean value of U_k^{A}, U_k^{B}, and U_k^{C}; γ_{MDV_k} expresses the voltage unbalance rate at node k. The distribution network operators should abide by the European Standard EN 50160 (2011) to keep the voltage unbalance ratio within 2% [31]. Once the ratio exceeds 2%, the fuse on one phase of a three-phase capacitor bank may be blown [32]. Therefore, when γ_{MDV_k} exceeds 2%, the aggregated ACs regulate the phase voltage unbalance in the distribution network [30]. The active power used to regulate the phase voltage unbalance is obtained using the PID algorithm, which can be expressed as:

$$P_{\mathrm{M}\_k}=KP\cdot e(t)+KI\cdot\sum e(t)+KD\cdot(e(t)-e(t-1)) \tag{23}$$

where KP, KI, and KD are the PID regulation coefficients; $e(t)$ is the difference between γ_{MDV_k} and the limit of the voltage unbalance rate (2%) at time slot t; P_{M_k} is the active power used to decrease γ_{MDV_k} at node k (W). The phase of P_{M_k} is dependent on Max $\{U_k^{\mathrm{A}}-U_k^{\mathrm{mean}},U_k^{\mathrm{B}}-U_k^{\mathrm{mean}},U_k^{\mathrm{C}}-U_k^{\mathrm{mean}}\}$.

V. AC CLUSTERING AND POWER MISMATCH ALLOCATION

The power-flow calculation can obtain the active power provided by the ACs. However, ACs cannot be uniformly dispatched to participate in voltage regulation because of their different operating states and parameters. However, during the operation, $\rho_{\mathrm{SOC\_AC}_i}$ obeys a certain probability distribution, which describes the potential of the AC's regulation ability. To optimize the regulation scheme and explore the AC regulation potential, ACs with similar regulation potential must be clustered into a group.

AP is a flexible clustering algorithm, which is not affected by data initialization [33]. In the process of clustering, the negative Euclidean distance between $\rho_{\mathrm{SOC\_AC}_x}$ and $\rho_{\mathrm{SOC\_AC}_y}$ indicates the similarity of the voltage regulation potential of the two ACs. The similarity equation can be expressed as:

$$s_{\mathrm{ap}}(x,y)=-\mathrm{d}^2(\rho_{\mathrm{SOC\_AC}_x},\rho_{\mathrm{SOC\_AC}_y})=-\|\rho_{\mathrm{SOC\_AC}_x}-\rho_{\mathrm{SOC\_AC}_y}\|^2 \quad x\neq y \tag{24}$$

where $s_{\mathrm{ap}}(x, y)$ is the similarity between the xth and yth AC's regulation potential; $\rho_{\mathrm{SOC\_AC}_x}$ is the thermal energy storage states of the xth AC. When x is equal to y, $s_{\mathrm{ap}}(x, x)$ expresses the ability of the xth AC as a cluster center. The value of $s_{\mathrm{ap}}(x, x)$ is larger, indicating that the yth AC has more potential to be the cluster center.

The AP algorithm obtains the cluster center by iterating responsibility and availability, which can be expressed as [33]:

$$r_{\mathrm{ap}}(x,y)\leftarrow s_{\mathrm{ap}}(x,y)-\max\{a_{\mathrm{ap}}(x,y')+s_{\mathrm{ap}}(x,y')\},\ y' \text{ s.t. } y'\neq y \tag{25}$$

$$a_{\mathrm{ap}}(x,y)\leftarrow\min\{0,r_{\mathrm{ap}}(y,y)+\sum_{x' \text{ s.t. } x'\notin\{x,y\}}\max\{0,r_{\mathrm{ap}}(x',y)\}\} \tag{26}$$

where $r_{\mathrm{ap}}(x, y)$ and $a_{\mathrm{ap}}(x, y)$ are the cumulative evidence and suitability, respectively, when the yth AC is the cluster center of the xth AC. If the value of the responsibility $r_{\mathrm{ap}}(x, y)$ is higher, the yth AC has a greater possibility of becoming a cluster center. The value of the availability $a_{\mathrm{ap}}(x, y)$ is higher, the yth and xth ACs are more likely to belong to the same category. When $x = y$, the $a_{\mathrm{ap}}(x, x)$ is set to self-availability, which reflects accumulated evidence that the xth AC is a cluster center. The accumulated evidence of the xth AC can be expressed as:

$$a_{\mathrm{ap}}(x,x)\leftarrow\sum_{x' \text{ s.t. } x'\neq x}\max\{0,r_{\mathrm{ap}}(x',x)\} \tag{27}$$

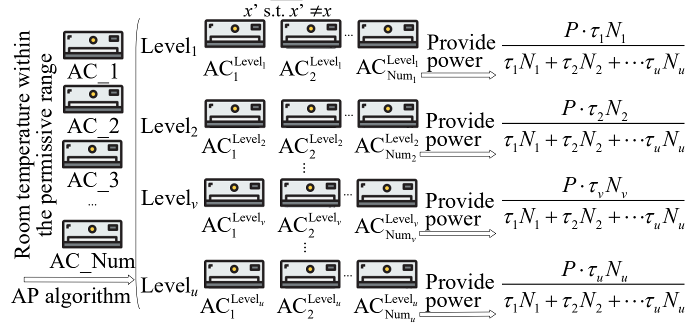

Fig. 5 Affinity propagation algorithm classifies the aggregated ACs

This article has been accepted for publication in IEEE Transactions on Power Delivery. This is the author's version which has not been fully edited and content may change prior to final publication. Citation information: DOI 10.1109/TPWRD.2022.3218658

The iterative process should consider the damping coefficient to avoid numerical oscillations. Therefore, the iterations of responsibility and availability can be expressed as:

$$r_{\mathrm{ap}_{t+1}}(x,y)=(1\text{-}\lambda)\cdot r_{\mathrm{ap}_{t+1}}(x,y)+\lambda\cdot r_{\mathrm{ap}_t}(x,y) \tag{28}$$

$$a_{\mathrm{ap}_{t+1}}(x,y)=(1\text{-}\lambda)\cdot a_{\mathrm{ap}_{t+1}}(x,y)+\lambda\cdot a_{\mathrm{ap}_t}(x,y) \tag{29}$$

where $r_{\mathrm{ap}_t}(x, y)$ and $r_{\mathrm{ap}_{t+1}}(x, y)$ are the responsibility before and after updating, respectively; $a_{\mathrm{ap}_{t+1}}(x, y)$ and $a_{\mathrm{ap}_t}(x, y)$ are the availabilities before and after updating, respectively; λ is the damping coefficient.

When the node voltage exceeds the permissive range, the ACs whose $\rho_{\mathrm{SOC\_AC}_i}$ is within 0–100% prepare to participate in voltage regulation. According to $\rho_{\mathrm{SOC\_AC}_i}$, the AP algorithm divides these ACs into u levels (Fig. 5).

Combining $\rho_{\mathrm{SOC\_AC}_i}$ and $H_{\max}$, the current heat storage capacity of the air-conditioned room can be calculated:

$$H_{\mathrm{AC}_i}=\rho_{\mathrm{SOC\_AC}_i}\cdot H_{\max} \tag{30}$$

The ACs in different levels will be aggregated to estimate the voltage regulation ability:

$$H_{\mathrm{cluster}_v}=\sum H_{\mathrm{AC}_i} \tag{31}$$

where H_{cluster_v} is the voltage regulation ability of the ACs in level v. When the voltage fluctuation leads to voltage problems, the ACs will be allocated active power adjustments based on the H_{AC_i} and clustering results. The AC allocation regulation power at level v can be expressed as:

$$P_{Level\_v}=\frac{P}{\tau_1\cdot N_1+\tau_2\cdot N_2+\cdots\tau_v\cdot N_v+\cdots\tau_u\cdot N_u}\cdot\tau_v\cdot N_v \tag{32}$$

where P_{Level_v} is the active power allocated to the AC in level v (W); $[N_1,N_2,\cdots N_v,\cdots,N_u]$ are the AC numbers at different levels; $[\tau_1,\tau_2,\cdots\tau_v,\cdots,\tau_u]$ are the regulation coefficients, which are related to the regulation level. A higher level has a larger regulation coefficient.

VI. Experiment Setup

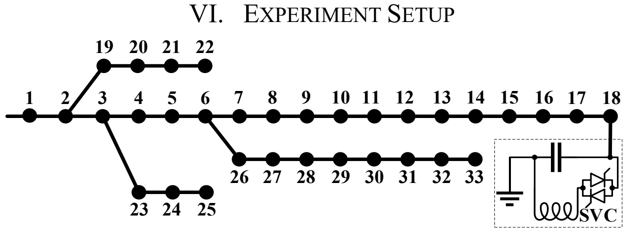

Fig. 6 IEEE 33-node power distribution system

We implement the improved Newton-Raphson power-flow algorithm by the MATLAB R2018a on a Win10-based i7-7820HK PC. An IEEE 33-node distribution network is used to demonstrate the validity of the improved Newton-Raphson power-flow algorithm (Fig. 6). Node 1 is the reference node, and the other nodes are all "PQ" nodes in the distribution network. The voltage of these nodes and the voltage unbalance rate should be controlled within 0.9–1.1 p.u. and 0%–2%, respectively [32]. The simulation time begins at 6:00 a.m. and lasts for one day. The duration of each slot is 30 s. The power-flow calculation and room temperature measurements are performed at the beginning of each slot.

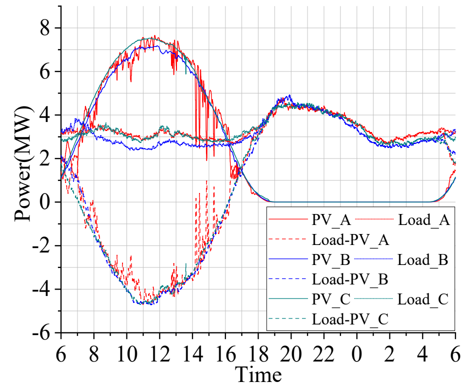

Fig. 7 Aggregated data of PVs and base load

TABLE II
Constant Parameter Initialization of the AC and Air-Conditioned Room

Symbol	Definition or description	Value	Units
Thermal model			
T_{in}	Temperature of the air-conditioned room	22–26	℃
T_{set}	Set temperature of AC	23–25	℃
R	Air-conditioned room's equivalent thermal resistance	N(2,0.1)	kWh/℃
Ca	Air's equivalent heat capacity	N(2,0.1)	J/℃
Electric model			
a	Coefficient of the cooling power equation	N(-378,10)	N/A
b	Coefficient of the cooling power equation	N(13608,800)	N/A
c	Coefficient of the cooling power equation	N(-17472,800)	N/A
m	Coefficient of the operating power equation	N(0.03,0.0005)	N/A
n	Coefficient of the operating power equation	N(-0.04,0.0005)	N/A
$f_{\mathrm{AC}}^{\min}$	Minimum operating frequency	30	Hz
$f_{\mathrm{AC}}^{\max}$	Maximum operating frequency	180	Hz
AP algorithm			
λ	Damping coefficient	0.5–1	N/A

* N(μ, σ) is a normal distribution whose mean and standard deviation is μ and σ, respectively;

A total of 300 occupants are assumed at each node of the IEEE 33-node power distribution network. Because node 18 is far from the reference point, the imbalance of generation and demand could easily cause severe voltage fluctuations. An SVC is installed at node 18, which has a power capacity of 3 × 300 kVA (capacitive) and 3 × 300 kVA (inductive). The slope of the SVC has 20 possible tap positions. Each occupant equips with AC, and 80% of occupants install PV generation. The ACs and PV generations are evenly connected in three phases. The related parameter initialization of the thermal model of the air-conditioned room, the electric model of the IAC, and the AP algorithm is shown in TABLE II. The PV and load data are obtained from [34]. Fig. 7 shows the aggregated data for each phase's loads and PVs. The PVs begin to generate at 5:00, and power generation increases continuously before noon. The PV generation of phases A, B, and C attaine the peaks at 11:42:00, 11:51:00, and 11:22:00, respectively. The peak PV generations of phases A, B, and C are 8.003, 7.184, and 7.566 MW, respectively. The loads of each phase fluctuate between 2.355 and 4.910 MW.

This article has been accepted for publication in IEEE Transactions on Power Delivery. This is the author's version which has not been fully edited and content may change prior to final publication. Citation information: DOI 10.1109/TPWRD.2022.3218658

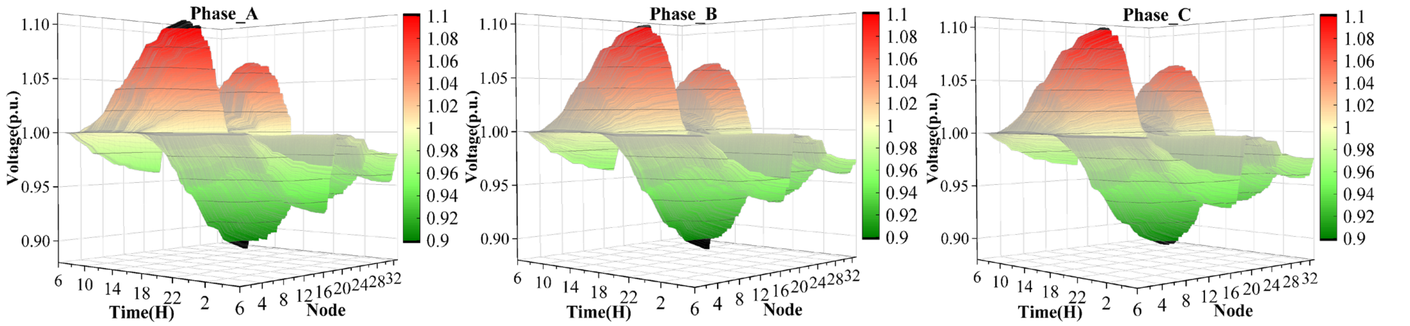

Fig. 8 Voltages of nodes before regulation in each phase

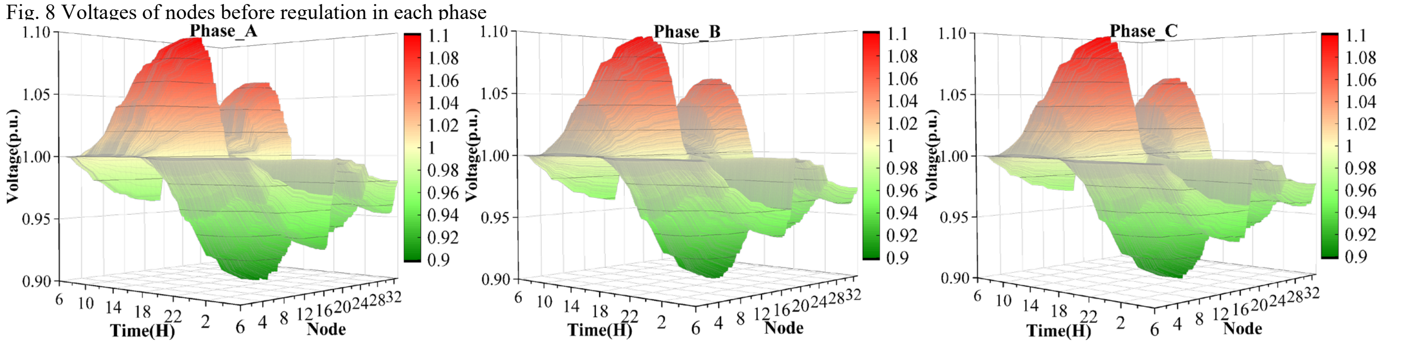

Fig. 9 Voltages of nodes after regulation in each phase

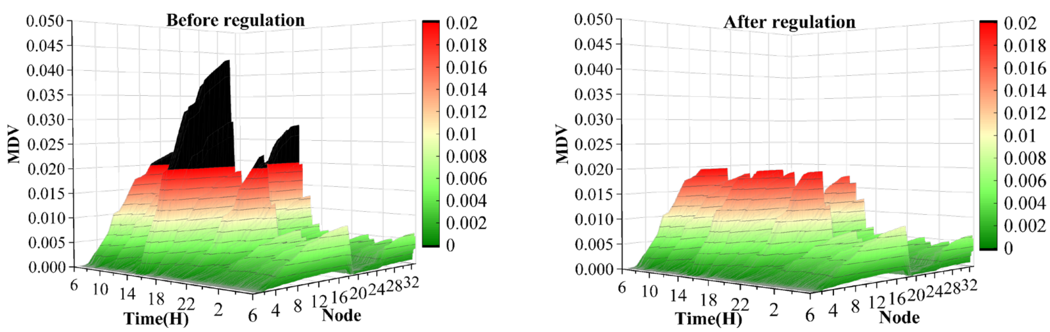

Fig. 10 γ_{MDV_k} of power distribution system before and after regulation

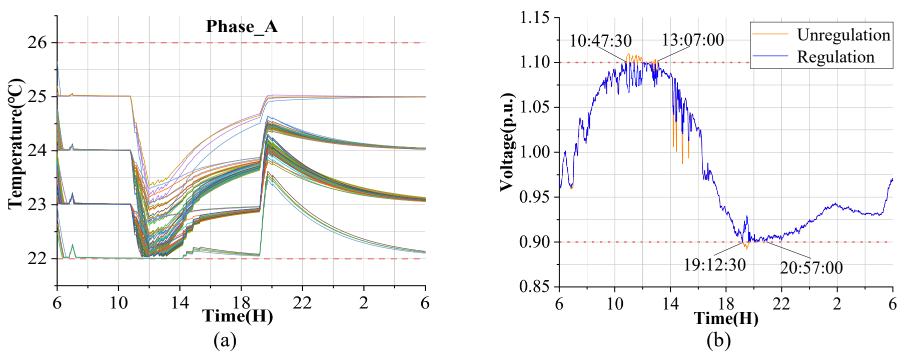

Fig. 11 (a) Room temperature curves of node 18 in phase A, (b) voltage curves of node 18 in phase A

VII. Numeric Test and Result Analysis

A. Nodal voltage without optimization

32 nodal voltage profiles of each phase are shown in Fig. 8. On the right of the figure are the color mappings of the voltage value. Once the nodal voltage is greater than 1.1 p.u. or less than 0.9 p.u., the profiles will turn to be black.

The over-voltage problem of phase A is the most severe, and the problem exists at nodes 14–18 from 10:47:30–13:07:00. The maximum voltage is 1.110 p.u. at 10:59:00. The under-voltage problem of phase B is the most severe, and the problem exists at nodes 14–18 from 19:07:30–20:36:00. The minimum voltage reaches 0.889 p.u. at 19:56:00.

B. Nodal voltage with optimization

The optimization algorithm will be implemented for voltage regulation when the nodal voltage exceeds the permissive range. When ACs provide voltage regulation, each phase voltage curve of the 32-node is shown in Fig. 9. All the nodal voltages keep in 0.9–1.1 p.u..

In phase A, the nodal voltage of node 18 attains 1.110 p.u. at 10:59:00, which is the highest value of the whole day. The ACs of this node increase 204.807 kW of operating power to decrease the nodal voltage to 1.067 p.u.. The nodal voltage of node 18 reaches 0.892 p.u. at 19:30:00, which is the lowest

This article has been accepted for publication in IEEE Transactions on Power Delivery. This is the author's version which has not been fully edited and content may change prior to final publication. Citation information: DOI 10.1109/TPWRD.2022.3218658

value of the whole day. The ACs of this node decrease 147.551 kW of operating power to increase the nodal voltage to 0.929 p.u..

In phase B, the nodal voltage of node 18 attains 1.103 p.u. at 11:29:00, which is the highest value of the whole day. The ACs of this node increase 189.421 kW of operating power to decrease the nodal voltage to 1.085 p.u.. The nodal voltage of node 18 reaches 0.889 p.u. at 19:56:00, which is the lowest value of the whole day. The ACs of this node decrease 148.444 kW of operating power to increase the nodal voltage to 0.933 p.u..

In phase C, the nodal voltage of node 18 attains 1.103 p.u. at 10:52:00, which is the highest value of the whole day. The ACs of this node increase 190.297 kW of operating power to decrease the nodal voltage to 1.084 p.u.. The nodal voltage of node 18 reaches 0.895 p.u. at 20:24:00, which is the lowest value of the whole day. The ACs of this node decrease 145.529 kW of operating power to increase the nodal voltage to 0.920 p.u..

C. Voltage unbalance optimization

The voltage unbalance rate of the power distribution system is shown in Fig. 10. Three-phase voltage unbalance occurs intermittently from 6:47:30–19:56:00, and node 18 is the most severely affected among all the nodes. γ_{MDV_k} is 0.0423 at 14:52:00. The voltages of phases A, B, C, and average are 0.987, 1.057, 1.048, and 1.031p.u., respectively. The difference between phase A and the average voltage is maximum. Therefore, the ACs reduce 101.764 kW of operating power in phase A. After regulation, the voltage increases to 1.042 p.u., and γ_{MDV_k} reduces to 0.0137.

D. Room temperature without/with the optimization

As shown in Figs. 8 and 10, the voltage problems are most severe in phase A. Therefore, when the ACs provide voltage regulation service, the room temperatures fluctuate widely. The room-temperature curves of node 18 in phase A are shown in Fig. 11(a). γ_{MDV_k} exceeds 2% intermittently during the period 6:47:30–19:56:00. The ACs provide active power when γ_{MDV_k} exceeds 2%. The room temperatures do not change significantly due to the short duration of the three-phase voltage unbalance.

The voltage curves of node 18 in phase A are shown in Fig. 11(b). In phase A, the over-voltage of node 18 occurs between 10:47:30–13:07:00. ACs increase their operating power. At the beginning of the regulation, all room temperatures are close to the set temperature. After ACs provide voltage regualtion service, the average room temperature and $\rho_{\mathrm{SOC\_AC}_i}$ are 22.402 °C and 0.8995, respectively. The maximum room temperature and $\rho_{\mathrm{SOC\_AC}_i}$ are 23.250 °C and 0.6875, respectively, and the minimum room temperature and $\rho_{\mathrm{SOC\_AC}_i}$ are 22.060 °C and 0.985, respectively. The under-voltage of node 18 occurs from 19:12:30–20:57:00. ACs decrease their operating power by decreasing compressors' operating frequency. At the beginning of the regulation, the room temperatures are close to the set temperature. After regulation, the average room temperature and $\rho_{\mathrm{SOC\_AC}_i}$ are 24.204 °C and 0.449, respectively, the maximum room temperature and $\rho_{\mathrm{SOC\_AC}_i}$ are 24.971 °C and 0.2573, respectively, and the minimum room temperature and $\rho_{\mathrm{SOC\_AC}_i}$ are 23.812 °C and 0.547, respectively.

E. The detailed optimal voltage regulation process

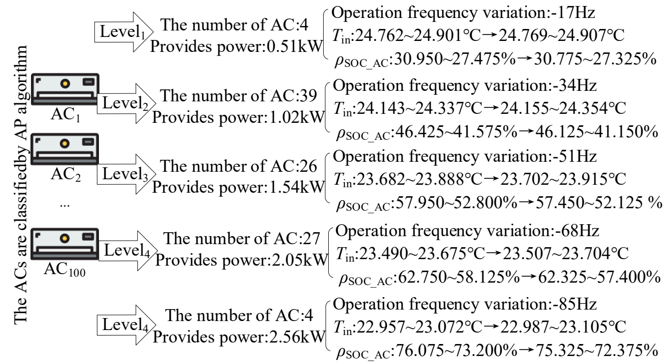

Fig. 12. The detailed optimal voltage regulation process of node 18

Fig. 12 shows the detailed optimal under-voltage regulation process of node 18. At 19:30:00, the voltage at node 18 of phase A is 0.892 p.u.. The ACs are required to decrease 147.551 kW of operating power to optimize the voltage to the permissible range. ACs with $\rho_{\mathrm{SOC\_AC}_i}$ higher than 0% are selected to provide voltage regulation service. These ACs are first sorted by the AP algorithm and fall into five categories. There are 4 ACs in Level 5, which have the most potential to provide voltage regulation service. These ACs provide the most active power among the 100 ACs. Each AC compressor decreases 85 Hz of operating frequency to provide 2.56 kW of active power. The room temperatures of these ACs before and after the regulation are 22.957–23.072 °C and 22.987–23.105 °C, respectively. The $\rho_{\mathrm{SOC\_AC}}$ of these ACs before and after the regulation are 76.075–73.200 and 75.325–72.375%, respectively. Level 4 has 27 ACs. Each AC compressor decreases 68 Hz of operating frequency to provide 2.05 kW of active power. The room temperatures of these ACs before and after the regulation are 23.490–23.675 °C and 23.507–23.704 °C, respectively. The $\rho_{\mathrm{SOC\_AC}}$ of these ACs before and after the regulation are 62.750–58.125 and 62.325–57.400%, respectively. Level 3 has 26 ACs. Each AC compressor decreases 51 Hz of operating frequency to provide 1.54 kW of active power. The room temperatures of these ACs before and after the regulation are 23.682–23.888 °C and 23.702–23.915 °C, respectively. The $\rho_{\mathrm{SOC\_AC}}$ of these ACs before and after the regulation are 57.950–52.800 and 57.450–52.125%, respectively. Level 2 has 39 ACs. Each AC compressor decreases 34 Hz of operating frequency to provide 1.02 kW of active power. The room temperatures of these ACs before and after the regulation are 24.143–24.337 °C and 24.155–24.354 °C, respectively. The $\rho_{\mathrm{SOC\_AC}}$ of these ACs before and after the regulation are 46.425–41.575 and 46.125–41.150%, respectively. Level 1 has 4 ACs. Each AC compressor decreases 17 Hz of operating frequency to provide 0.51 kW of active power. The room temperatures of these ACs before and after the regulation are 24.762–24.901 °C and 24.769–

This article has been accepted for publication in IEEE Transactions on Power Delivery. This is the author's version which has not been fully edited and content may change prior to final publication. Citation information: DOI 10.1109/TPWRD.2022.3218658

24.907 °C, respectively. The ρ_{SOC_AC} of these ACs before and after the regulation are 30.950–27.475 and 30.775–27.325%, respectively. The regulated active power depends on the cluster results. All room temperatures are within the comfortable range.

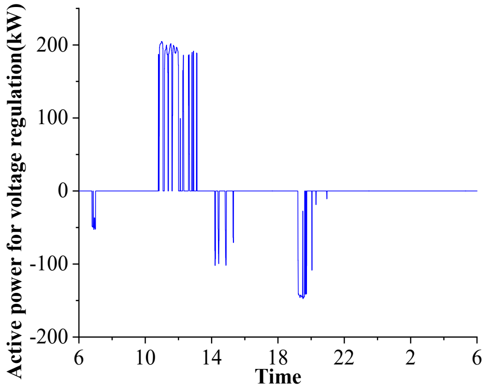

Fig. 13 Active power for voltage regulation service

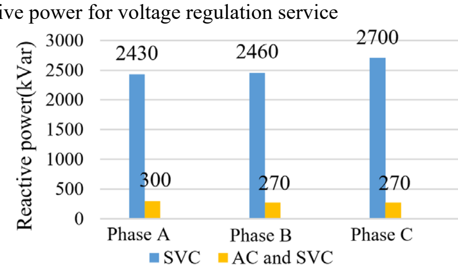

Fig. 14 Capacity of SVC to provide voltage regulation service alone, and capacity of SVC assisting ACs in voltage regulation

F. *Saving of the IAC for voltage regulation*

The active power curves provided by the ACs for the voltage regulation of node 18 in phase A are shown in Fig. 13. The battery model of the IAC discharge time is 56 min, and the electricity is released at 93.167 kWh. The charging time is 77 min, and 236.782 kWh of electricity is absorbed. The price of the lithium battery is estimated to be $100/kWh [35]. Therefore, the IACs substitute the battery for providing voltage regulation service, which can aid in saving the occupants more than $23,678.22.

G. *SVC participating in auxiliary regulation*

The finite ACs cannot deal with all the problems of voltage violation. However, ACs can provide voltage regulation services with other equipment. In this case, the penetration of the PVs increases by 15%, and after ACs participate in voltage regulation, overvoltage and voltage unbalance problems still exist. Subsequently, the SVCs in node 18 provide a voltage regulation service in the reactive power control mode [4]. At 12:00:00, the voltage of phase A reaches a maximum of 1.111 p.u. The SVC absorbs 270 kVar of reactive power to decrease the voltage to 1.096 p.u.. At 14:11:00, the voltage unbalance rate reaches a maximum of 0.0236, and the SVC provides 150 kVar of reactive power to decrease the unbalance rate to 0.0184. As shown in Fig. 14, compared with the voltage regulation provided by the SVC alone, ACs aides in reducing the capacity of the SVC. When only the SVC participates in voltage regulation, an SVC with a 7590 kVar capacity should have been installed in node 18. When the ACs participate in voltage regulation with the SVC, an SVC with only an 840 kVar capacity should have been installed in node 18. Therefore, ACs can be used as voltage regulation equipment to reduce the capacity of SVC.

VIII. Conclusions

In this paper, the IACs are used as energy storage batteries for the voltage regulation of a distribution network. The thermoelectric model of the IAC is modeled to formulate a room's thermal dynamic variation. Based on this model, the IAC is equivalent to the energy storage battery, which can make IACs compatible with existing dispatch model BESS. AP is used to cluster ACs with different states and parameters. The different clusters provide different active powers to utilize the regulation potential of the ACs fully. The simulation and results show that the equivalent model of the IAC has a similar performance to the battery. Similar to the charging /discharging of the battery, the ACs can provide different active powers by changing their operating frequency to maintain the nodal voltage and voltage unbalance rate within 0.9–1.1 p.u. and 0.02, respectively. The maximum/minimum voltage of the distribution network increases and decreases from 1.110 and 0.889 p.u. to 1.067 and 0.933 p.u., respectively, and the maximum γ_{MDV_k} decreases from 0.0423 to 0.0137. During voltage regulation, the smart controller monitors and controls the equivalent battery's SOC and room temperature, which are maintained in the ranges of 0.257–0.985 and 22.060–24.971 °C, reducing the effect of voltage regulation on occupants. Moreover, substituting the battery with the AC in the voltage regulation aids occupants to save more than $23,678.22 for the investment of regulation equipment in node 18. In summary, the IAC has a great potential to participate in regulation services in distribution networks.

This paper has filled a gap in voltage regulation using IACs in a three-phase power distribution network. Electrical quality can be increased by controlling the IACs to provide voltage regulation services for the distribution network. In addition, our future research will focus on developing a control strategy for a hybrid energy storage model, which includes a single-speed air conditioner, an IAC, and an energy storage battery.

References

[1] Y. Che, S. Xue, W. He, H. Bi, and L. Liu, "A Three-Phase Allocation Strategy Solving Three-Phase Unbalance Problem in Air Conditioners' Applications," *2019 22nd Int. Conf. Electr. Mach. Syst. ICEMS 2019*, pp. 1–5, 2019.

[2] M. Chamana and B. H. Chowdhury, "Optimal Voltage Regulation of Distribution Networks With Cascaded Voltage Regulators in the Presence of High PV Penetration," *IEEE Trans. Sustain. Energy*, vol. 9, no. 3, pp. 1427–1436, 2018.

[3] J. Liu *et al.*, "An OLTC-inverter coordinated voltage regulation method for distribution network with high penetration of PV generations," Int. J. Electr. Power Energy Syst., vol. 113, no. May, pp. 991–1001, 2019.

[4] N. Daratha, B. Das, and J. Sharma, "Coordination between OLTC and SVC for voltage regulation in unbalanced distribution system distributed generation," IEEE Trans. Power Syst., vol. 29, no. 1, pp. 289–299, 2014.

[5] C. Long and L. F. Ochoa, "Voltage control of PV-rich LV networks: OLTC-fitted transformer and capacitor banks," IEEE Trans. Power Syst., vol. 31, no. 5, pp. 4016–4025, 2016.

[6] E. Rivas, J. C. Burgos, and J. C. García-Prada, "Vibration analysis using envelope wavelet for detecting faults in the OLTC tap selector," IEEE Trans. Power Deliv., vol. 25, no. 3, pp. 1629–1636, 2010.

[7] F. Bai, R. Yan, and T. K. Saha, “A New Remote Tap Position Estimation Approach for Open-Delta Step-Voltage Regulator in a Photovoltaic Integrated Distribution Network,” IEEE Trans. Power Syst., vol. 33, no. 4, pp. 4433–4443, 2018.

[8] R. A. Walling, R. Saint, R. C. Dugan, J. Burke, and L. A. Kojovic, “Summary of distributed resources impact on power delivery systems,” IEEE Trans. Power Deliv., vol. 23, no. 3, pp. 1636–1644, 2008.

[9] A. Mishra and V. N. Kumar Gundavarapu, “Line utilisation factor-based optimal allocation of IPFC and sizing using firefly algorithm for congestion management,” IET Gener. Transm. Distrib., vol. 10, no. 1, pp. 115–122, 2016.

[10] S. Ghosh, S. Rahman, and M. Pipattanasomporn, “Distribution Voltage Regulation Through Active Power Curtailment With PV Inverters and Solar Generation Forecasts,” IEEE Trans. Sustain. Energy, vol. 8, no. 1, pp. 13–22, 2017.

[11] F. Wang, J. L. Duarte, and M. A. M. Hendrix, “Pliant active and reactive power control for grid-interactive converters under unbalanced voltage dips,” IEEE Trans. Power Electron., vol. 26, no. 5, pp. 1511–1521, 2011.

[12] R. Deng, Z. Yang, M. Y. Chow, and J. Chen, “A survey on demand response in smart grids: Mathematical models and approaches,” IEEE Trans. Ind. Informatics, vol. 11, no. 3, pp. 570–582, 2015.

[13] H. Hui, Y. Ding, Q. Shi, F. Li, Y. Song, and J. Yan, “5G network-based Internet of Things for demand response in smart grid: A survey on application potential,” Appl. Energy, vol. 257, no. August 2019, p. 113972, 2020.

[14] L. Gomes, J. Spínola, Z. Vale, and J. M. Corchado, “Agent-based architecture for demand side management using real-time resources’ priorities and a deterministic optimization algorithm,” J. Clean. Prod., vol. 241, 2019.

[15] S. Sharda, M. Singh, and K. Sharma, “Demand side management through load shifting in IoT based HEMS: Overview, challenges and opportunities,” Sustain. Cities Soc., vol. 65, no. October 2020, p. 102517, 2021.

[16] A. E. Onile, R. Machlev, E. Petlenkov, Y. Levron, and J. Belikov, “Uses of the digital twins concept for energy services, intelligent recommendation systems, and demand side management: A review,” Energy Reports, vol. 7, pp. 997–1015, 2021.

[17] T. Karthick, S. Charles Raja, J. Jeslin Drusila Nesamalar, and K. Chandrasekaran, “Design of IoT based smart compact energy meter for monitoring and controlling the usage of energy and power quality issues with demand side management for a commercial building,” Sustain. Energy, Grids Networks, vol. 26, p. 100454, 2021.

[18] N. Iliopoulos, M. Esteban, and S. Kudo, “Assessing the willingness of residential electricity consumers to adopt demand side management and distributed energy resources: A case study on the Japanese market,” Energy Policy, vol. 137, no. December 2018, p. 111169, 2020.

[19] A. K. Barik and D. C. Das, “Coordinated regulation of voltage and load frequency in demand response supported biorenewable cogeneration-based isolated hybrid microgrid with quasi-oppositional selfish herd optimisation,” Int. Trans. Electr. Energy Syst., vol. 30, no. 1, pp. 1–22, 2020.

[20] H. Yang, S. Tang, Z. Zeng, X. He, R. Zhao, and M. Kuroda, “Demand response of inverter air conditioners and applications in distribution system voltage stability enhancement,” 2013 Int. Conf. Electr. Mach. Syst. ICEMS 2013, no. Dlc, pp. 954–959, 2013.

[21] H. Hui, P. Siano, Y. Ding, P. Yu, Y. Song, H. Zhang and N. Dai, “A Transactive Energy Framework for Inverter-based HVAC Loads in a Real-time Local Electricity Market Considering Distributed Energy Resources,” IEEE Trans. Industrial Informatics, vol. 18, no. 12, pp. 8409-21, 2022.

[22] M. Song, C. Gao, H. Yan, and J. Yang, “Thermal battery modeling of inverter air conditioning for demand response,” IEEE Trans. Smart Grid, vol. 9, no. 6, pp. 5522–5534, 2018.

[23] H. Hui, Y. Chen, S. Yang, H. Zhang and T. Jiang, “Coordination Control of Distributed Generators and Load Resources for Frequency Restoration in Isolated Urban Microgrids,” Appl. Energy, vol. 327, p. 120116, 2022.

[24] Y. Che, J. Yang, Y. Zhou, Y. Zhao, W. He, and J. Wu, “Demand Response From the Control of Aggregated Inverter Air Conditioners,” IEEE Access, vol. 7, pp. 88163–88173, 2019.

[25] D. Ryder-cook, “Thermal Modelling of Buildings,” U-Value, pp. 1–23, 2009.

[26] M. Lakeridou, M. Ucci, A. Marmot, and I. Ridley, “The potential of increasing cooling set-points in air-conditioned offices in the UK,” Appl. Energy, vol. 94, pp. 338–348, 2012.

[27] Y. Hua, X. Shentu, Q. Xie, and Y. Ding, “Voltage / Frequency Deviations Control via Distributed Battery Energy Storage System Considering State of Charge,” Appl. Sci., vol. 9, 2019.

[28] T. Ding, C. Li, Y. Yang, R. Bo, and F. Blaabjerg, “Negative Reactance Impacts on the Eigenvalues of the Jacobian Matrix in Power Flow and Type-1 Low-Voltage Power-Flow Solutions,” IEEE Trans. Power Syst., vol. 32, no. 5, pp. 3471–3481, 2017.

[29] N. C. Yang and H. C. Chen, “Decomposed Newton algorithm-based three-phase power-flow for unbalanced radial distribution networks with distributed energy resources and electric vehicle demands,” Int. J. Electr. Power Energy Syst., vol. 96, no. November 2017, pp. 473–483, 2018.

[30] M. T. Bina and A. Kashefi, “Three-phase unbalance of distribution systems: Complementary analysis and experimental case study,” Int. J. Electr. Power Energy Syst., vol. 33, no. 4, pp. 817–826, 2011.

[31] C. Oramas-Piero, E. Vega-Fuentes, and F. Deniz, “Genetic algorithm based control for unbalanced low voltage networks,” 2018 110th AEIT Int. Annu. Conf. AEIT 2018, pp. 1–4, 2018.

[32] Institute of Electrical and Electronics Engineers, IEEE Std 1159 - IEEE Recommended Practice for Monitoring Electric Power Quality., vol. 2009, no. June. 2009.

[33] B. J. Frey and D. Dueck, “Clustering by passing messages between data points,” Science (80-.)., vol. 315, no. 5814, pp. 972–976, 2007.

[34] Q. Xie, R. Hara, H. Kita, and E. Tanaka, “Coordinated Control of OLTC and Multi-CEMSs for Overvoltage Prevention in Power Distribution System,” IEEJ Trans. Electr. Electron. Eng., vol. 12, pp. 692–701, 2017.

[35] “Analysis of lithium battery industry chain in 2021.” 2021.< https://www.qianzhan.com/analyst/detail/220/210304-9dadfd66.html >

Yongzhu Hua received the B.S. degree from Hangzhou Dianzi University Information Engineering College, Zhejiang, China, in 2014. He received the M.S. and Ph.D. degrees from Hangzhou Dianzi University, Zhejiang, China, in 2017 and 2021, respectively. He is currently a Postdoctoral Researcher of Hangzhou Dianzi University, Hangzhou, China. His current research interests include voltage control of distribution network and control of flexible resources.

Qiangqiang Xie received the B.S. and M.S. degrees from University of Electronic Science and Technology of China, Chengdu, China, in 2009 and 2012, respectively. He received the Ph.D. degree from Hokkaido University, Sapporo, Japan, in 2017. He is currently a lecturer of Hangzhou Dianzi University, Hangzhou, China. His current research interests include voltage control of distribution network and demand side management.

Hongxun Hui received the B.E. and Ph.D. degrees in electrical engineering from Zhejiang University, Hangzhou, China, in 2015 and 2020, respectively. He is currently a Research Assistant Professor with the State Key Laboratory of Internet of Things for Smart City, University of Macau, Macao SAR, China. His current research interests include power system optimization, demand-side resource control, and Internet of Things technologies for smart energy.

Yi Ding received the B.S. degree in electrical engineering from Shanghai Jiaotong University, Shanghai, China, in 2000, and the Ph.D. degree in electrical engineering from Nanyang Technological University, Singapore, in 2007. He is currently a Professor with the College of Electrical Engineering, Zhejiang University, Hangzhou, China. His research interests include power systems reliability and performance analysis incorporating renewable energy resources, and engineering systems reliability modeling and optimization.

Jiadong Cui received the B.S. degree from Hangzhou Dianzi University, Zhejiang, China, in 1997 and the M.S. degree from Zhejiang University, Zhejiang, China, in 2005. He is currently an associate Professor of Hangzhou Dianzi University, Hangzhou, China. His current research interests include Internet of Things and industrial control.

Lihuan Shao received the B.S. and the M.S. degree from Hangzhou Dianzi University, Zhejiang, China, in 2004 and 2008, respectively. He is currently an associate Professor of Hangzhou Dianzi University, Hangzhou, China. His current research interests include switching mode power supply and embedded system.